Excitation of mercury atoms in nitrogen post-discharge

To cite this article: F Krma *et al* 2014 *J. Phys.: Conf. Ser.* **516** 012005

View the article online for updates and enhancements.

Related content

IOP ebooks™

Bringing you innovative digital publishing with leading voices to create your essential collection of books in STEM research.

Start exploring the collection - download the first chapter of every title for free.

Excitation of mercury atoms in nitrogen post-discharge

F Krčma[1], I Bocková[1], V Mazánková[1], I Soural[1], A Hrdlička[2], V Kanický[2]

[1] Faculty of Chemistry, Brno University of Technology, Purkyňova 118, 612 00 Brno, Czech Republic
[2] Faculty of Science, Masaryk University, Kotlářská 2, 611 37 Brno, Czech Republic

E-mail: krcma@fch.vutbr.cz

Abstract. The work presents results obtained during spectroscopic observations of nitrogen DC flowing post-discharges at the total gas pressure of 1000 Pa and at the discharge current of 100 mA. Mercury traces were introduced into the system using auxiliary pure nitrogen flow enriched by mercury vapor. A very low mercury concentration of 3.7 ppb was introduced into the system before the active discharge. The strong quenching of nitrogen pink afterglow was observed but no mercury lines were recorded. Moreover, the vibrational distributions of nitrogen excited states were nearly unchanged. Based on these results, the new experimental set up was created. The introduction point of mercury vapor with higher concentration of 600 ppm was movable during the post discharge up to decay time of 40 ms. Besides three nitrogen spectral systems (first and second positive and first negative), NO^β and NO^γ bands, the mercury line at 254 nm was recorded at these conditions. Its intensity was dependent on the mercury vapor introduction position as well as on the mercury concentration. No other mercury lines were observed. The creation of mercury $^3P_1$ state that is the upper state of the observed mercury spectral line is possible by the resonance excitation energy transfer form vibrationally excited nitrogen ground state $N_2(X\ ^1\Sigma_g^+,\ v = 19)$. The observed results should form a background for the development of a new titration technique used for the highly vibrationally excited nitrogen ground state molecules determination.

1. Introduction

Nitrogen post-discharges in various configurations have been subjects of many studies during last fifty years [1-6]. Besides laboratory and technological plasmas, the nitrogen post-discharge is studied also in the kinetics of upper Earth atmosphere (corona borealis [7-9]) and these processes are also taken into account in some extraterrestrial systems, for example in Titan atmosphere [10, 11]. The neutral nitrogen molecule can form many electronic states. Due to its symmetry, all vibrational levels of the ground state $N_2(X\ ^1\Sigma_g^+)$ and also the first eight levels of the first electronically excited state $N_2(A\ ^3\Sigma_u^+)$ are metastables. Besides them, there are some other strongly metastable highly excited states (a' $^1\Sigma_u^-$ – 67 739 cm^{-1} and a $^1\Pi_g$ – 68 951 cm^{-1} [12]). All these states conserve the excitation energy for very long time. The excitation energy transfer during the collisions among these species as well as atomic recombination processes lead to formation of some radiative states and the visible light emission can be observed up to one second after switching off an active discharge depending on the experimental conditions, mainly on pressure and nitrogen purity.

The first period (up to about 3 ms) of the post-discharge in the pure nitrogen is characterized by a

strong decrease of the light emission. After that, the strong light emission at the decay time of about 5–14 ms after the end of an active discharge, known as a pink afterglow, can be observed [13, 14] (for photography see in [15]). The pink afterglow is manifested by a strong increase of the pink light emission at the decay times of about 6–8 ms in pure nitrogen, while the yellow-orange color is characteristic for the other parts of the nitrogen afterglow. The nitrogen pink afterglow can be characterized as a secondary discharge because the electron concentration strongly increases due to various collisionally induced ionization processes [16, 17], and thus many discharge properties are similar to those in the active discharge. The electron density measurements during the afterglow show the strong increase of the free electron concentration during this post-discharge period [18]. The effect of the nitrogen pink afterglow can be studied only in nitrogen of very high purity; various traces (especially carbon traces and oxygen traces) quench it [19, 20]. The present work extends our experiments of the nitrogen post-discharge kinetics changes caused by mercury impurity [15]. A simplified kinetic model of the post-discharge processes running in the studied system is given, too.

2. Experimental setup
The DC flowing post-discharge was used for the experimental study. A simplified schematic drawing of the experimental setup is given in figure 1.
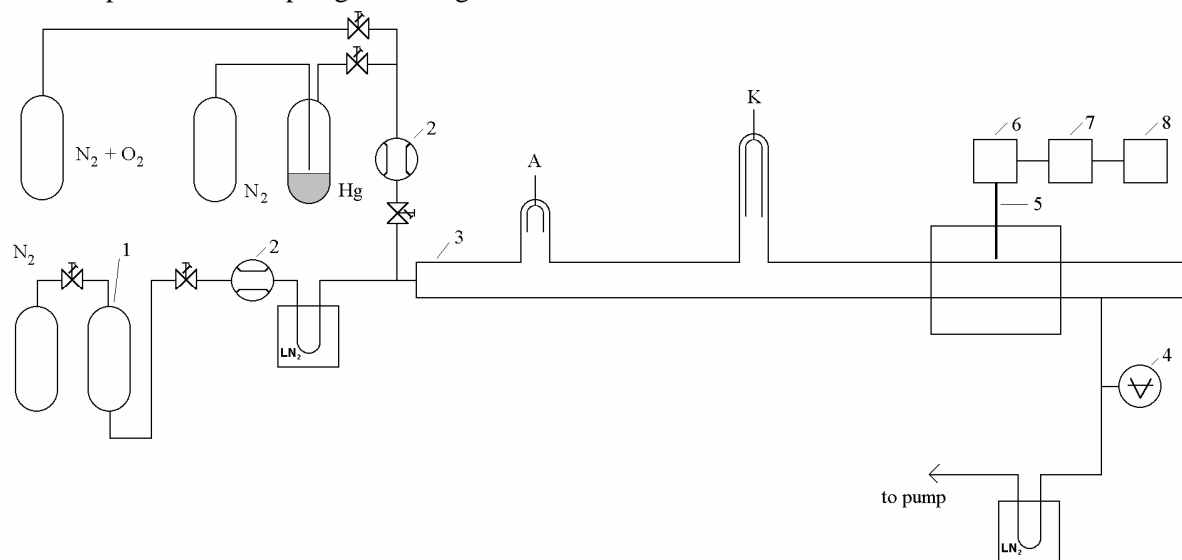
Figure 1: A simplified scheme of the experimental setup: 1 – catalyzer Oxiclear; 2 – mass flow controller; 3 – Pyrex/Quartz discharge tube (900 mm long, inner diameter of 13 mm); 4 – capacitance gauge; 5 – quartz optical fiber; 6 – monochromator Jobin Yvon Triax 550; 7 – CCD; 8 – PC.

The active discharge was created in a Pyrex or Quartz discharge tubes with a 120 mm electrode distance at current of 100 mA and pressure of 1000 Pa. Hollow molybdenum electrodes were placed in the side arms of the main discharge tube to minimize their sputtering and also to suppress the light emitted in the electrode regions. Nitrogen was of 99.999%–99.9999% purity and it was further cleaned by Oxiclear and LN_2 traps. No oxygen or carbon traces were detectable in the pure nitrogen discharge (concentrations under 1 ppm and 0.01 ppm, respectively [20, 21]). The reactor system was pumped continuously by a rotary oil pump separated from discharge tube by another LN_2 trap to suppress oil back flow and keep high nitrogen purity needed for the experiments.

A sealed PE test tube with liquid Hg of 99.995% purity was purged with the pure N_2 flux of 7.5 ml min^{-1} ensuring a saturated Hg vapor (0.2 µg min^{-1} Hg at laboratory temperature of 30 °C in a steady state). The mercury vapor condensation was observed in the MFC valve which controlled its flow into the discharge. Due to this fact, a special procedure was developed to verify the exact quantity of mercury in the discharge [15]. The mercury vapor concentration in the discharge was determined as

(3.70 ± 0.05) ppb. As some oxygen traces were detected in the mercury flow, the synthetic air was used to verify the oxygen influence. The appropriate oxygen concentration of 528 ppm was calculated using the spectra of NO^{β} system (see correlation presented in figure 5).

The spectra of post-discharge were measured by Jobin Yvon monochromator TRIAX 550 with the 1200 grooves per mm grating coupled with CCD multichannel detector. The emitted light was led to the entrance slit of the monochromator by the multimode quartz optical fiber movable along the discharge tube without any cut off optical filters. The optical fiber holder (length of 6 cm, optical fiber is mounted at its center) had to be filled by liquid nitrogen. Thus the reactor wall temperature was possible to cool down of 77 K around ($\pm$ 3 cm) the observation point. The temperature of decaying plasma was calculated as 400 K at the ambient wall temperature and 100 K at liquid nitrogen wall temperature using the simulated nitrogen 1st positive ($N_2(B\,^3\Pi_g) \to (A\,^3\Sigma_u^+)$) 2-0 band spectrum [22].

Nitrogen 1st ($N_2(B\,^3\Pi_g) \to (A\,^3\Sigma_u^+)$) and 2nd ($N_2(C\,^3\Pi_u) \to (B\,^3\Pi_g)$) positive and nitrogen 1st negative ($N_2^+(B\,^2\Sigma_u^+) \to (X\,^2\Sigma_g^+)$) systems were recorded in all spectra. The bands of NO^{β} system (NO $(B\,^2\Pi)$ $\to$ $NO\,(X\,^2\Pi)$) and NO^{γ} system (NO $(A\,^2\Sigma^+)$ $\to$ $NO\,(X\,^2\Sigma)$) systems dominantly originating at vibrational level 0 were observed, too. No other molecular emissions were observed. Further, no mercury lines were recorded during the discharge or post-discharge in the measured spectral region of 300–800 nm even in quartz tube. The relative vibrational populations at the selected nitrogen levels were calculated using all measurable emission band intensities. The transition probabilities and wavelengths of the transitions were taken from *Gilmore's* tables [23].

3. Results

Populations at the selected vibrational levels are presented in figures 2–4 as a function of decay time and wall temperature. The pink afterglow effect is well visible in all cases in pure nitrogen. At the decreased wall temperature, the pink afterglow maximum is displaced for longer time, in comparison to the afterglow at the ambient temperature and its maximal emission takes of about 10 ms duration. The molecular ion $N_2^+(B\,^2\Sigma_u^+)$ population (see figure 4) decrease during the post-discharge after pink afterglow is about one order higher than for the other states.
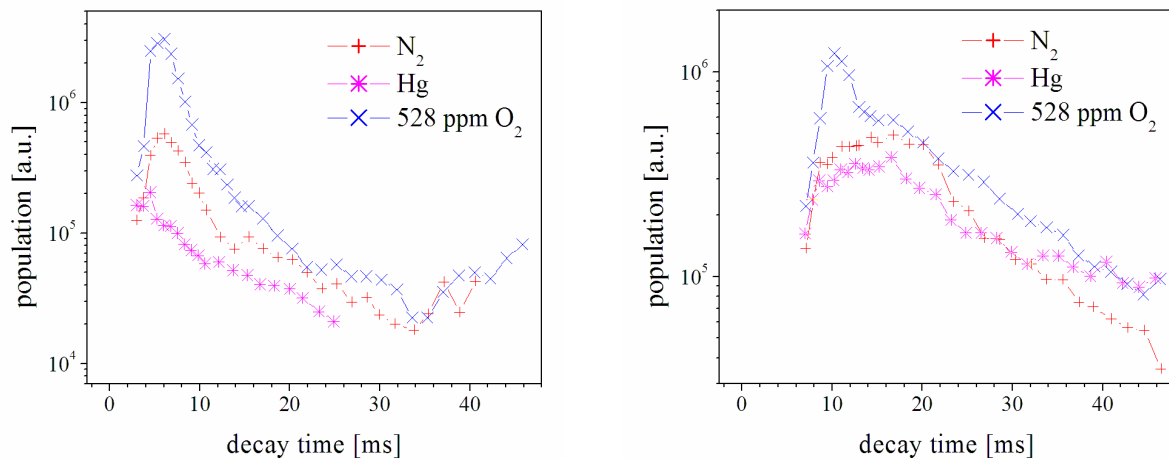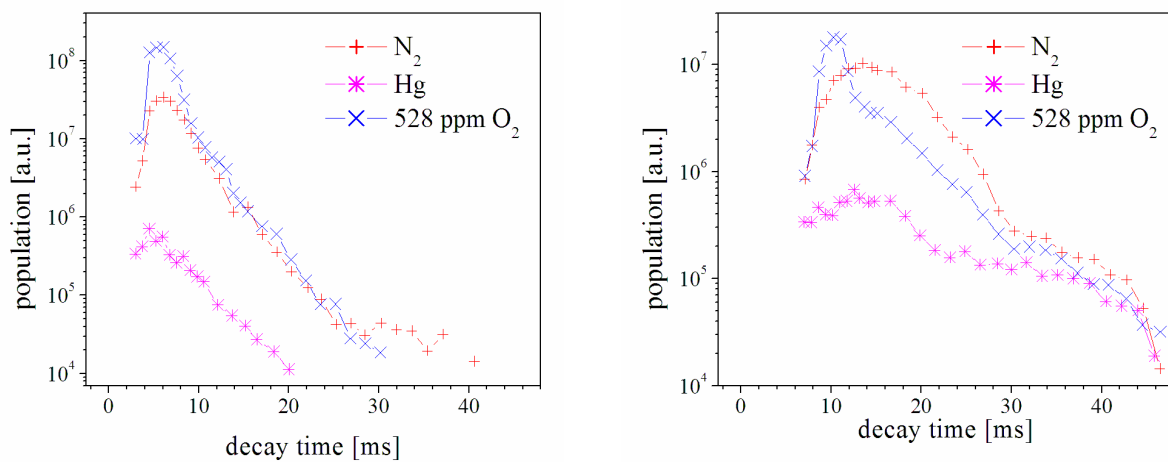

Figure 2: Population profiles at the $N_2\,(C\,^3\Pi_u,\, v = 0)$ vibrational level during the post-discharge in pure nitrogen and pure nitrogen containing traces of oxygen and mercury at the ambient (left) and liquid nitrogen (right) wall temperatures.

The most visible effect of oxygen presence is strong enhancement of the pink afterglow emission. The maximum is about five times higher than in pure nitrogen and it is strongly located in short time interval between 10 and 13 ms. After that, the populations of neutral nitrogen states show nearly the same dependence as in the pure nitrogen, only the populations are slightly higher. The population of molecular ionic state is lower than in pure nitrogen in the time interval of 13–30 ms, after that the population is nearly the same as in pure nitrogen.
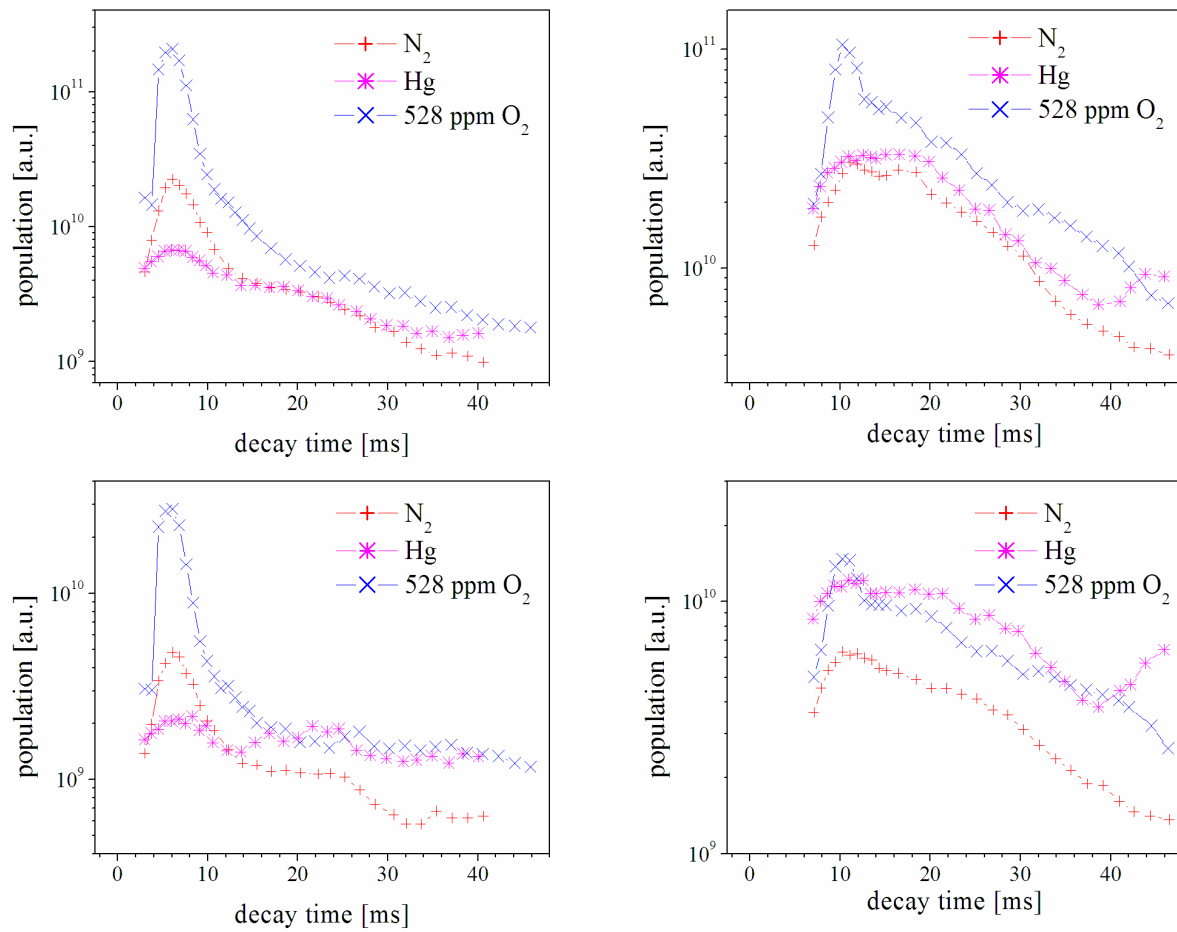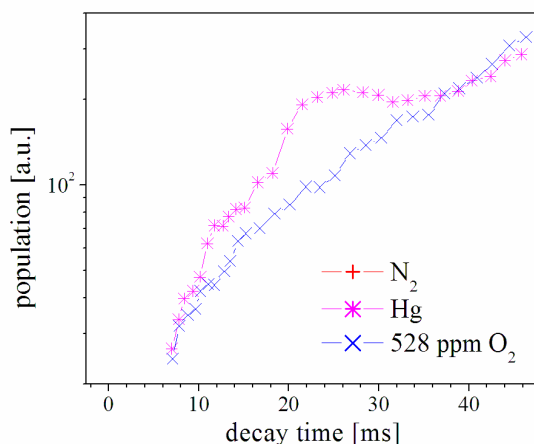
Figure 3: Population profiles at the vibrational levels 2 (top) and 11 (bottom) of N_2 (B $^3\Pi_g$) state during the post-discharge in pure nitrogen and pure nitrogen containing traces of oxygen and mercury at the ambient (left) and liquid nitrogen (right) wall temperatures. The vibrational levels are selected by the main mechanisms of their population – see the section 4.

Figure 4: Population profiles at the molecular ionic N_2^+ (B $^2\Sigma_u^+$, v = 0) level during the post-discharge in pure nitrogen and pure nitrogen containing traces of oxygen and mercury at the ambient (left) and liquid nitrogen (right) wall temperatures.

The situation is completely changed when mercury traces are added. The pink afterglow effect is nearly the same or slightly more intensive as in pure nitrogen at lower N_2 (B $^3\Pi_g$) state levels, at levels over the predissociation limit (v > 12) as well as in the N_2 (C $^3\Pi_u$) state the pink afterglow is slightly quenched. The populations at levels just under the predissociation limit, i.e. levels N_2 (B $^3\Pi_g$, v = 11 and 12) show the significant increase of populations in the time interval of 10–12 ms but not such strong as in nitrogen-oxygen mixture. After that the populations are even the highest among the studied gas mixtures. The population increase at the later decay times in the case of all vibrational levels of N_2 (B $^3\Pi_g$) state is surprising. The profile of molecular ion population shows strong pink afterglow quenching, the populations at pink afterglow position is more than one order lower than in pure nitrogen. But at the latest decay times over 30 ms, the populations are nearly the same as in the other gas mixtures.

The intensities of NO^β bands are presented in figure 5. No data are available for the pure nitrogen due to its really high purity. Although the dependencies in the decay time interval of 10–35 ms are different, the figure 5 shows that the oxygen presence in mercury flow was well estimated. The difference of both dependencies should be caused by the increase of nitrogen dissociation by mercury atoms or by some other process (probably mainly wall processes) that increases the atomic nitrogen particles concentrations.


Figure 5: Intensity profile of the NO^β 0-8 band head during the post-discharge in pure nitrogen and pure nitrogen containing traces of oxygen and mercury at liquid nitrogen wall temperature.

The vibrational distributions of N_2 (B $^3\Pi_g$) state are presented in figure 6 at three selected decay times. The distributions show the same results as presented in figure 3. The vibrational distributions are nearly the same in all three gas mixtures at the earliest afterglow. At the pink afterglow maximum (middle figures), the distributions in pure nitrogen and in N_2-Hg mixture are generally the same, only at levels 11 and 12 the population is significantly higher when mercury is added; the populations in nitrogen-oxygen mixture are significantly higher at all levels. In later afterglow, the populations at higher levels (v > 12) are increased by oxygen but quenched by mercury. At lower levels (v < 13) the populations are increased by both oxygen and mercury. The population enhancement by mercury increases with the increase of decay time and at later times it is higher than the increase caused by oxygen.

4. Kinetic model

The nitrogen afterglow kinetics is a really complicated problem. The mechanisms that populate the radiative states of a neutral molecule and a molecular ion are different and they must be discussed separately. Further, the kinetics in both nitrogen mixtures is discussed. The main processes populating the observed states are schematically given in figure 7. The kinetic model was proposed recently [15] but some additions to this model are included as a result of the experimental data given in the last section.
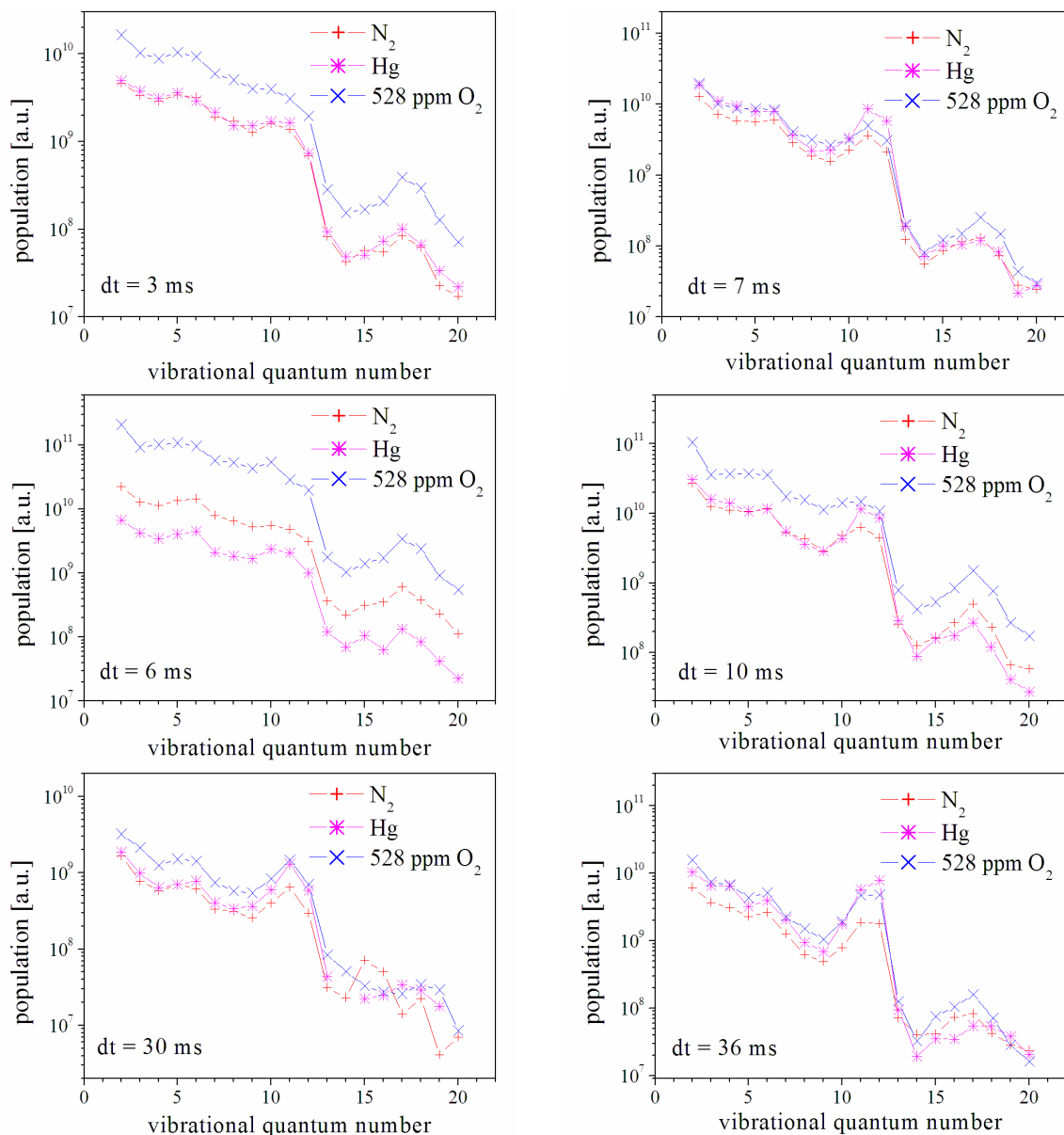
Figure 6: The vibrational distributions of the $N_2(B\,^3\Pi_g)$ state during the post-discharge. The upper figures correspond to the position between the active discharge and pink afterglow maximum; middle figures describe distribution at the pink afterglow maximum; bottom figures correspond to the late post-discharge. Distributions at ambient (left) and liquid nitrogen (right) wall temperatures are shown. (dt marked in figures means the decay time)

4.1 Neutral nitrogen

The $N_2(B\,^3\Pi_g)$ and $N_2(C\,^3\Pi_u)$ states are dominantly created by pooling reactions of lower metastable states, especially by the vibrational excited ground state and by the lowest 8 levels of $N_2(A\,^3\Sigma_u^+)$ state [2-4, 20]. The higher ground state vibrational levels populated by v-v process are also precursors for $N_2(A\,^3\Sigma_u^+)$ state creation because its concentration at the end of the active discharge is not high enough [13, 24]. The contribution of other metastable states, especially metastable singlet states, to the pink afterglow creation is not fully understood. Besides pooling reactions, the atomic nitrogen ground states three body recombination significantly contributes to vibrational populations, mainly at levels $N_2(B\,^3\Pi_g,\ v = 10\text{--}12)$. More complex description of the mechanisms was given recently [13, 25].
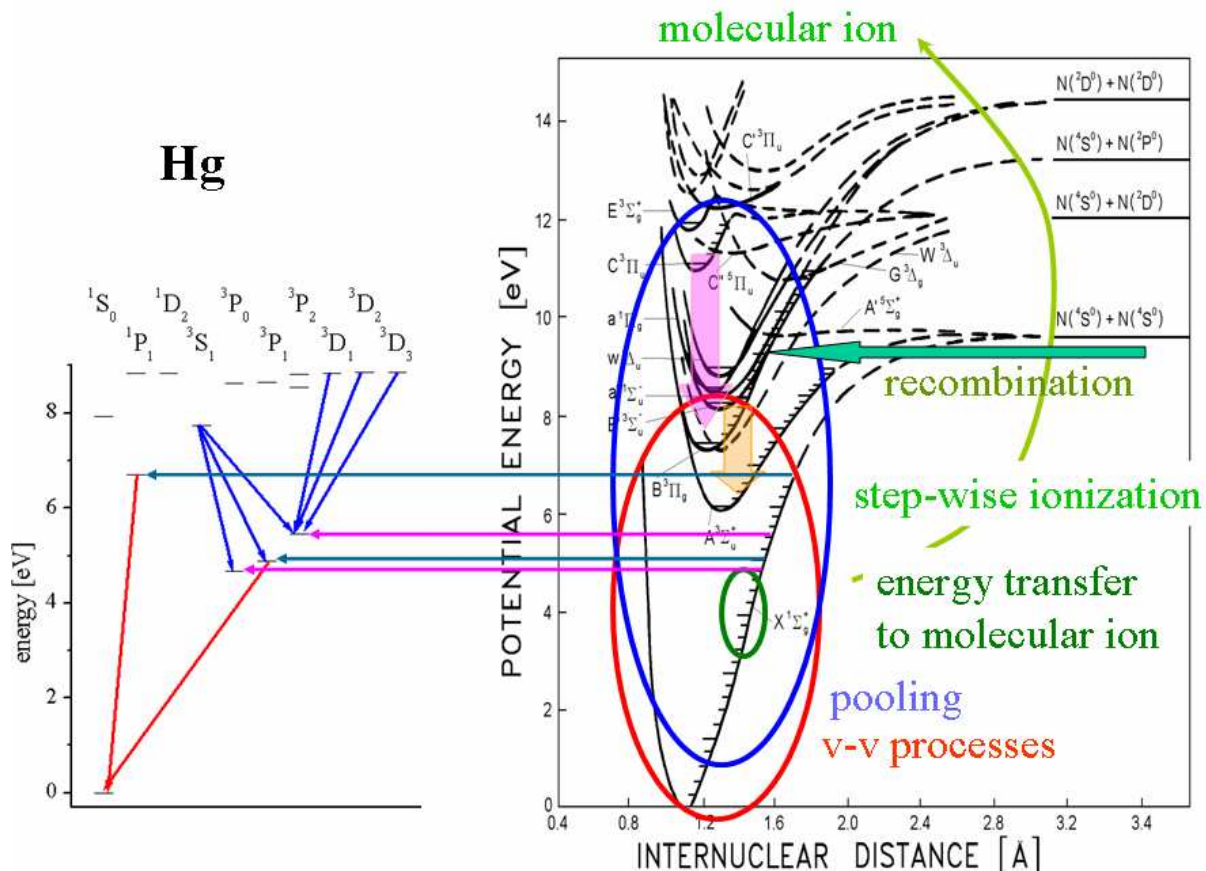
Figure 7: Scheme of kinetic processes among selected mercury and nitrogen states [15] (based on energies given by [12, 27]).

4.2 Nitrogen molecular ion

The kinetics of the molecular ion radiative state is more complicated and it can be explained in a two-step scheme. The charged particles concentration is very low before the pink afterglow [18], but during the pink afterglow it significantly increases. So the first step is the molecular ion creation. This process is known as a step-wise ionization [16, 17]. In its principle, the highly excited neutral metastable molecules (excited both electronically and vibrationally) can have energy sufficient for the ionization during their mutual collisions. After molecular ion creation, the excitation to the radiative state must be completed. Recent studies have demonstrated that the main process responsible for the population of the radiative $N_2^+ (B\ ^2\Sigma_u^+)$ state is the collisionally induced energy transfer from the vibrationally excited neutral ground state [21].

4.3 Nitrogen with oxygen traces

Kinetics of pure nitrogen with a small addition of oxygen can be generally described by the following simplified scheme. The first process is atomic recombination that forms the NO (B $^2\Pi$) state, preferentially at vibrational level v = 0. This state is an origin of the measured NO$^\beta$ spectral system. The NO can be effectively back dissociated during collisions with nitrogen ground state molecules excited at least to level v = 13. This process significantly influences the v-v pumping in nitrogen and thus the formation of electronically excited nitrogen states is quenched. The influence on formation of the lowest $N_2 (B\ ^3\Pi_g)$ levels is smaller because they can be formed during collisions of lower vibrationally excited ground states. The formation of nitrogen molecular ion is strongly decreased, too, and thus the nitrogen 1st negative system is effectively quenched. High vibrationally excited ground state nitrogen molecules (over v = 22) can also excite the NO species into the NO $(A\ ^2\Sigma^+)$ state that is
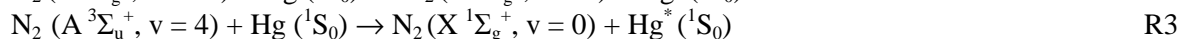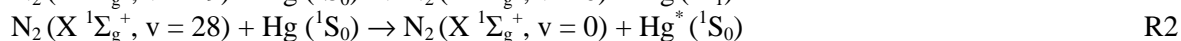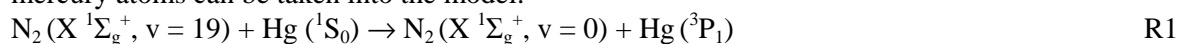
an origin of NO^γ spectral system. Such process was confirmed by our observations but the results are not presented here. The NO dissociation leads to the increase of atomic nitrogen concentration during the post-discharge. This process is confirmed by the enhancement of populations at $N_2 (B\ ^3\Pi_g$, v = 10–12) levels in the nitrogen-oxygen gas mixture.

The reactions with molecular oxygen can be neglected because we can assume high molecular oxygen dissociation in an active discharge (the residence time of about 8 ms) and the recombination forming molecular oxygen during the afterglow can be neglected due to its low concentration.

4.4 Nitrogen with mercury traces

The influence of mercury atoms on the post-discharge kinetics is more simple because the mercury atomic energy levels lay mostly at higher energies (see figure 7) where nitrogen molecular states are not metastable, and thus their populations are very low. Due to this fact no mercury lines from visible and near UV part of the spectrum (marked by blue arrows in figure 7) were observed. Thus only the following reactions (marked by dark blue arrows in figure 7) between nitrogen metastables and mercury atoms can be taken into the model.

$$N_2 (X\ ^1\Sigma_g^+,\ v = 19) + Hg\,(^1S_0) \rightarrow N_2 (X\ ^1\Sigma_g^+,\ v = 0) + Hg\,(^3P_1) \qquad\qquad R1$$

$$N_2 (X\ ^1\Sigma_g^+,\ v = 28) + Hg\,(^1S_0) \rightarrow N_2 (X\ ^1\Sigma_g^+,\ v = 0) + Hg^*\,(^1S_0) \qquad\qquad R2$$

$$N_2 (A\ ^3\Sigma_u^+,\ v = 4) + Hg\,(^1S_0) \rightarrow N_2 (X\ ^1\Sigma_g^+,\ v = 0) + Hg^*\,(^1S_0) \qquad\qquad R3$$

Reaction R1 leads to the formation of the excited $Hg\,(^3P_1)$ mercury state that is the origin of the resonance line at the wavelength of 254 nm. R2 and R3 reactions produce the excited mercury $^1S_0$ state that is the origin of the resonance line at 185 nm. Both these allowed transitions are marked as red arrows in figure 7. The experimental data presented in previous section do not confirm these reactions directly. R1 and R2 reactions partially stop the v-v processes in the nitrogen ground state, R3 reaction leads to the depopulation of $N_2 (A\ ^3\Sigma_u^+)$ state. Thus the pooling reactions or step-wise ionization processes could not efficiently create highly excited electronic states of nitrogen and pink afterglow is quenched. The production of the lowest $N_2 (B\ ^3\Pi_g)$ vibrational levels is possible by the reactions of lower excited ground state metastables that are not influenced by mercury presence, and thus it is possible to observe some remains of the pink afterglow at these levels (see figure 3).

The other channels originating from adjacent metastable nitrogen vibrational levels could play some role but they are not creating any radiative states. These reactions are marked by magenta arrows in figure 6.

5. Introduction of mercury directly into the post-discharge

The new experimental device was built up based on the precedent results. This new set up allows introduction of mercury vapor at higher concentration (contemporary up to 600 ppm) directly into the selected post-discharge positions (i.e. at different decay times) using a thin capillary in the post-discharge tube oriented from the pumping side. Thus there is no influence on the discharge and post-discharge up to the mercury introduction position. To introduced mercury vapor the auxiliary pure nitrogen flow was used.

The emission of mercury line at 254 nm was observed as it is demonstrated by figure 8 where mercury line is recorded in the spectrum of the second order. No mercury emission was observed at the earlier decay times (before the introduction point) as it is demonstrated by figure 9. It can be also seen that there is about 2 ms delay between the mercury introduction and mercury line presence. After very fast increase of mercury line emission, relatively fast decrease of its intensity can be observed; the peak takes about 5 ms. The mercury line intensity remains more or less independent on the decay time behind this peak. The same mercury line emission profile was observed at all post-discharge positions but it was slightly different at the introduction positions before the pink afterglow. This is probably directly connected to the kinetics of $N_2 (X\ ^1\Sigma_g^+,\ v = 19)$ precursor state. The other proposed mercury line (at 185 nm) was never recorded during the experiments up to now.
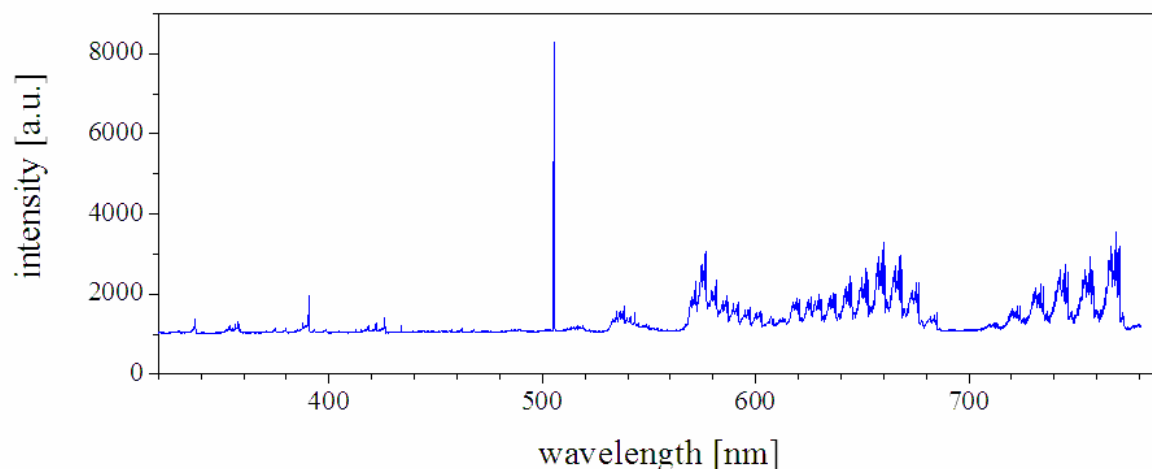
Figure 8: Example of nitrogen post-discharge spectrum at the decay time of 31 ms with mercury line at 254 nm observed in the second order spectrum. Mercury was introduced at decay time of 28.5 ms.
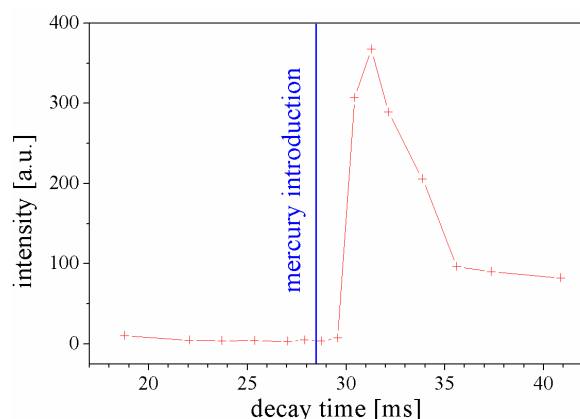
Figure 9: Mercury 254 nm line intensity during the post-discharge at selected position of mercury introduction.
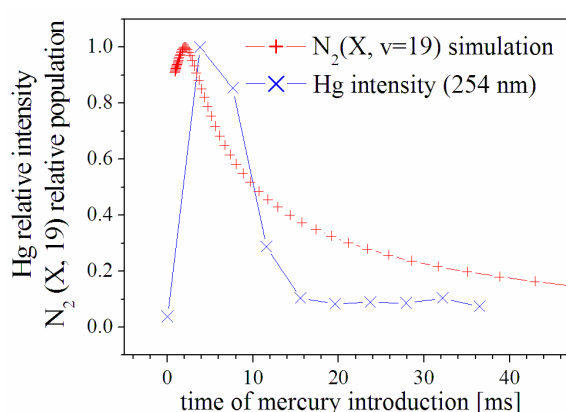
Figure 10: Comparison of mercury line maximal intensity at different positions of introduction and calculated population of precursor nitrogen state.

As we proposed in the kinetic model, the mercury line at 254 nm should directly reflect the concentration of its precursor, i.e. concentration of $N_2(X\,{}^1\Sigma_g^+,\,v = 19)$ molecules. To confirm this hypothesis, we measured maximal mercury line intensity from response peaks ~~like~~ as it is presented in figure 9 as a function of the mercury introduction position into the post-discharge. The result is presented by a blue curve in figure 10. The obtained mercury intensity profile is compared to the calculated concentration of the precursor nitrogen state. The qualitative agreement is well visible in figure 10. The correspondence is not ideal due to two main facts. First of all, the time resolution of mercury line response peak (see figure 9) is limited and thus the maximal intensity presented in figure 10 could not fully reflect the real maximum of mercury line intensity peak. The second problem is that mercury amount was fixed and thus it is not sure if it was possible to reflect the precursor concentration correctly. The last experiments showed that the mercury line intensity was directly proportional to its concentration at low mercury concentrations but saturation effect was observed. The saturation should be reached to obtain a good correlation between mercury line intensity and nitrogen metastable precursor concentration. The proposal that mercury titration into the post-discharge should be used for the monitoring of highly vibrationally excited nitrogen ground state concentration should be a conclusion of these most recent experiments.

6. Conclusions

The influence of mercury traces on the pure nitrogen post-discharge kinetics was experimentally studied in the DC flowing afterglow in Pyrex and Quartz reactors at ambient and decreased wall temperatures. It was confirmed that mercury de-excites the $N_2 (X\ ^1\Sigma_g^+, v = 19)$ vibrational level, the second proposed process de-exciting higher metastables was not confirmed, yet. Thus nitrogen v-v processes and various pooling reactions are not effective enough to create the nitrogen pink afterglow effect. The mercury spectral line at 254 nm was observed at the mercury titration directly into the post-discharge using higher mercury concentration. The correlation between mercury line maximal intensity and population at nitrogen precursor level was confirmed. Based on these results the possible way for monitoring of nitrogen metastables was proposed.

References

[1] Beale G E and Broida H P 1959 *J. Chem. Phys.* **31** 1030-1034
[2] Piper L G 1988 *J. Chem. Phys.* **88** 231-239
[3] Piper L G 1988 *J. Chem. Phys.* **88** 6911-6921
[4] Piper L G 1989 *J. Chem. Phys.* **91** 864-873
[5] Guerra V, Sa P A and Loureiro J 2001 *J. Phys. D, Appl. Phys.* **34** 1745-1755
[6] Krčma F 2005 *Acta Phys. Slovaca* **55** 453-460
[7] Lie-Svendsen Ø, Rees M H, Stamnes K and Whipple E C 1991 *Planet. Space Sci.* **39** 929-943
[8] Kirillov A S and Aladjev G A 1995 *Adv. Space Res.* **16** 105-108
[9] Morrill J S and Benesch W M 1996 *J. Geophys. Res. Space Phys.* **101** 261-274
[10] Keller C N, Anicich V G and Cravens T E 1998 *Planet. Space Sci.* **46** 1157
[11] Dimitrov V and Bar-Nun A 2004 *Prog. Reac. Kin. Mechanisms* **29** 1-41
[12] Lofthus A and Krupenie PH 1977 *J. Phys. Chem. Ref. Data* **6** 113-307
[13] Sa P A, Guerra V, Loureiro J and Sadeghi N 2004 *J. Phys. D, Appl. Phys.* **37** 221-231
[14] Loureiro J, Sa P A and Guerra V 2006 *J. Phys. D, Appl. Phys.* **39** 122-125
[15] Kanický V, Otruba V, Hrdlička A, Krásenský P and Krčma F *Journal of Atomic Analytical Spectrometry* **22**, 754-760
[16] Polak L S, Slovetskii D I and Sokolov A S 1972 *Opt. Spectrosc.* **32** 247-251
[17] Paniccia F, Gorse C, Cacciatore M and Capitelli M 1987 *J. Appl. Phys.* **61** 3123-3126
[18] Janča J, Tálský A and El Kattan N 1978 *Folia Physica* **27** 23-36
[19] Krčma F and Babák L 1999 *Czech. J. Phys.* **49** 271-288
[20] Krčma F, Mazánková V and Soural I 2007 *Publications of the Astronomical Observatory of Belgrade* **82**, 133-147
[21] Krčma F and Protasevich E T 2003 *Post-discharges in Pure Nitrogen and in Nitrogen Containing Halogenated Hydrocarbon Traces* (Tomsk: Tomsk Polytechnic University Publishing)
[22] Krčma F, Mazánková V, Soural I and Šimek M 2007 *Proc. Int. Conf. on Phenomena in Ionized Gases* (Prague 2007) pp 1722-1725
[23] Gilmore F R, Laher R R and Espy P J 1992 *J. Phys. Chem. Ref. Data* **21** 1005-1107
[24] Pintassilgo C D, Loureiro J and Guerra V 2005 *J. Phys. D, Appl. Phys.* **38** 417-430
[25] Sadeghi N, Foissac C and Supiot P 2001 *J. Phys. D, Appl. Phys.* **34** 1779-1788
[26] NIST Atomic Spectra Database: http://physics.nist.gov/PhysRefData/ASD/index.html